Transient thermal characterization of suspended monolayer MoS_2

Robin J. Dolleman,[1] David Lloyd,[2] Martin Lee,[1] J. Scott Bunch,[2,3] Herre S. J. van der Zant,[1] and Peter G. Steeneken[1,4,*]

[1]*Kavli Institute of Nanoscience, Delft University of Technology, Lorentzweg 1, 2628 CJ, Delft, The Netherlands*

[2]*Department of Mechanical Engineering, Boston University, Boston, Massachusetts 02215, USA*

[3]*Boston University, Division of Materials Science and Engineering, Brookline, Massachusetts 02446, USA*

[4]*Department of Precision and Microsystems Engineering, Delft University of Technology, Mekelweg 2, 2628 CD, Delft, The Netherlands*

(Received 21 June 2018; revised manuscript received 12 October 2018; published 26 November 2018)

We measure the thermal time constants of suspended single-layer molybdenum disulfide drums by their thermomechanical response to a high-frequency modulated laser. From this measurement, the thermal diffusivity of single-layer MoS_2 is found to be 1.14×10^{-5} m^2/s on average. Using a model for the thermal time constants and a model assuming continuum heat transport, we extract thermal conductivities at room temperature between 10 to 40 $W\,m^{-1}\,K^{-1}$. Significant device-to-device variation in the thermal diffusivity is observed. Based on a statistical analysis we conclude that these variations in thermal diffusivity are caused by microscopic defects that have a large impact on phonon scattering but do not affect the resonance frequency and damping of the membrane's lowest eigenmode. By combining the experimental thermal diffusivity with literature values of the thermal conductivity, a method is presented to determine the specific heat of suspended 2D materials, which is estimated to be 255 ± 104 $J\,kg^{-1}\,K^{-1}$ for single-layer MoS_2.

DOI: 10.1103/PhysRevMaterials.2.114008

I. INTRODUCTION

The distinct electronic [1–3] and mechanical [4,5] properties of atomically thin molybdenum disulfide open up possibilities for novel nanoscale electronic [6] and optoelectronic [7–9] devices. The large and tunable Seebeck coefficient of single-layer MoS_2 makes this material interesting for on-chip thermopower generation and thermal waste energy harvesting [10]. Since the power efficiency of these devices depends on the thermal conductivity, it is of interest to study the transport of heat in single-layer MoS_2. Several theoretical works have found values of the thermal conductivity k of single-layer MoS_2 ranging between $k = 1.35$ up to 83 $W\,m^{-1}\,K^{-1}$ [11–15]. By exploiting the temperature-dependent phonon frequency shifts in Raman spectroscopy [16], several experimental works have measured the thermal conductivity of single-layer MoS_2. Experimental values of $k = 34.5$ and 84 $W\,m^{-1}\,K^{-1}$ of exfoliated single-layer MoS_2 have been reported [17,18], while single-layer MoS_2 grown by chemical vapor deposition was found to show a significantly lower thermal conductivity of 13.3 $W\,m^{-1}\,K^{-1}$ [19].

Here, we thermally characterize suspended single-layer MoS_2 drum resonators by measuring their thermal time constants. This was achieved by measuring the frequency-dependent vibration amplitude in response to a sinusoidally varying heat flux delivered by a modulated diode laser, similar to previously reported characterization on single-layer graphene [20]. Since these are frequency-based measurements, the result is to first order independent of the absorbed laser power, which greatly facilitates calibration compared to Raman spectroscopy based methods. With respect to prior studies of thermal transport in single-layer MoS_2 [17–19] the current work determines the thermal conductivity of this 2D material using a different method, which helps to resolve the large controversy between the previously obtained values of this parameter. In addition, the study obtains the transient thermal time constant of the material, which is closely related to the phonon dynamics and thermalization, but can also provide information on thermomechanical dissipation mechanisms in 2D materials [21]. Furthermore, the method allows one to study relations between the mechanical and thermal properties of the material. From measurements of the thermal time constant τ, we find the thermal diffusivity of MoS_2 to be on average 1.05×10^{-5} m^2/s for 5 μm diameter drums and 1.29×10^{-5} m^2/s for 8 μm drums. Assuming a specific heat value of 373 $J\,kg^{-1}\,K^{-1}$, this corresponds to $k = 19.8$ and 24.7 $W\,m^{-1}\,K^{-1}$.

The remainder of this article is structured as follows. Section II describes the experimental setup, fabrication, actuation, and read-out of the motion of the single-layered MoS_2 drums. The following section, Sec. III, describes the thermal model of the system and how τ is extracted from the experiments. Section IV shows the experimental results of τ and extracts the value of the thermal diffusivity. This section also examines the relationship between mechanics and thermal transport. Section V contains an extensive discussion on several subjects. First, we compare the present results to single-layer graphene. Second, the relation between the mechanical and thermal properties is discussed. The third subject is the device-to-device spread observed in this work and we end the discussion with the specific heat of MoS_2. The conclusions of this work are then outlined in Sec. VI.

II. EXPERIMENTAL SETUP

We use a substrate with many circular cavities to perform the experiment. The fabrication starts with a silicon chip with

*Corresponding author: P.G.Steeneken@tudelft.nl

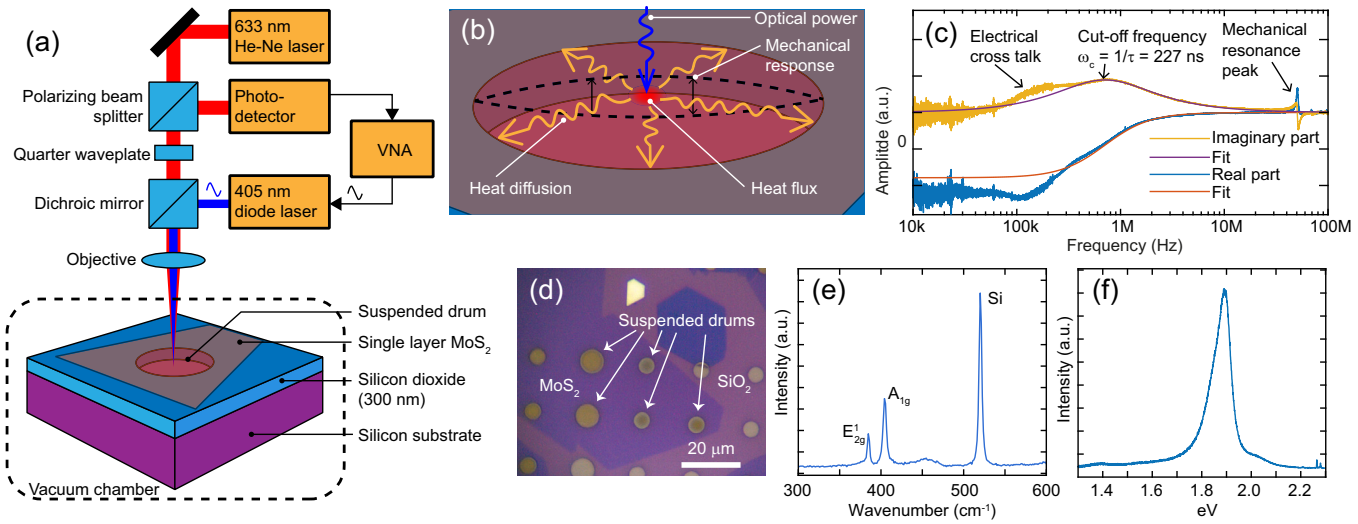

FIG. 1. (a) Schematic of the samples and the laser interferometer setup to actuate and detect the motion of the single-layer MoS_2 drum resonators. (b) Overview of the physical processes involved in measuring the transient properties of heat transport in the drum. (c) Typical experimental result of the real (in-phase) and imaginary (out-of-phase) part of the amplitude of the mechanical response of the drum. The imaginary part of the amplitude was fitted to Eq. (3) to find the thermal time constant. At lower frequencies, a feature due to electrical crosstalk becomes visible due to the low optical gain during the experiment (see Ref. [22]). At higher frequencies, the fundamental resonance is clearly visible. (d) Optical image of the device showing a single-layer MoS_2 sheet on top of the substrate and several suspended drums. (e) Raman spectrum of the suspended MoS_2. (f) Photoluminescence spectrum of the suspended MoS_2. The A^0 peak position is found at 1.89 eV.

285 nm of silicon dioxide. Circular cavities approximately 300 nm deep and with a diameter of 8 and 5 μms are etched in the oxide layer. Many single-layer MoS_2 flakes grown by chemical vapor deposition are transferred over the substrate by a dry transfer method using PMMA as a transfer polymer [23–25] to create suspended drum resonators as drawn in Fig. 1(a). After transfer, the sample was annealed in vacuum with argon gas at a temperature of 340 °C for 6 hours to reduce polymer contamination. An optical image of several devices is shown in Fig. 1(d). The Raman and photoluminescence (PL) spectra of the MoS_2 flakes are shown in Figs. 1(e) and 1(f), data were taken on suspended drums to prevent the effects of substrate doping [9,26,27]. These measurements ensure that the MoS_2 flakes are single layer, since no indirect transition is observed in the PL spectrum [Fig. 1(f)] [27]. In the Raman spectrum [Fig. 1(e)], the E^1_{2g} peak is found at 384.9 cm^{-1} and the A_{1g} peak at 404.5 cm^{-1}, also in accordance with single-layer MoS_2 [28]. Furthermore, the positions of both the E^1_{2g} Raman peak and PL A^0 (1.89 eV) suggests that no large strains (>1%) are induced by the transfer [25]. More details on the CVD growth and transfer can be found in Ref. [24]. The samples are kept in an atmosphere with a maximum pressure of 1×10^{-6} mbar for two weeks before and during the experiment to ensure all gas has escaped from the cavity.

Figure 1(a) also shows a schematic drawing of the interferometer setup used to actuate and read-out the motion of the membrane. The red laser intensity on the photodiode is used to read-out the motion using Fabry-Perot interferometry between the moving membrane and the fixed back mirror, which is the silicon [4,29,30]. The blue laser heats up the membrane, which causes the membrane to move due to thermal expansion [20,31]. The blue laser is power modulated using the output of a vector network analyzer (VNA). The input of the VNA is connected to the photodiode that detects the reflected red laser intensity. A dichroic mirror is used to prevent the blue laser light from reaching the photodiode. The VNA measures both the amplitude and the phase of the transmitted signal. All parasitic phase shifts in the electrical and optical components are measured by directly pointing the blue laser at the photodetector and are eliminated by using the measured transmission function to deconvolve the experimental results [20].

During the measurement of the parasitic phase shifts, a blue laser power of 2.35 mW with a sinusoidal ac-power modulation of 1 mW was used, but during experimental characterization, a neutral density filter reduced the optical power (measured before the objective) of the blue laser to 0.10 mW to prevent damage to the sample. The red laser power to probe the mechanical motion was set at 0.17 mW. A beam expander with a pinhole after the red laser ensures a Gaussian beam with an estimated waist diameter of 671 nm for the red laser spot in the focal point of the objective. The blue laser diode is coupled to a single-mode fiber, also resulting in a Gaussian beam with a waist diameter of 569 nm. Both lasers were aligned to the center of the drums during the experiments.

III. THERMAL TIME CONSTANT

Due to the diffusion of heat through the membrane, there will be a time delay between the optical power delivered to the membrane and the membrane's motion [Fig. 1(b)]. The diffusion of heat can be described by the heat equation:

$$\rho c_p \frac{dT}{dt} - k\nabla^2 T = P, \tag{1}$$

where $T(\mathbf{x}, t)$ is the temperature and $P(\mathbf{x}, t)$ the heat flux applied to the membrane. ρ is the density of the material, c_p

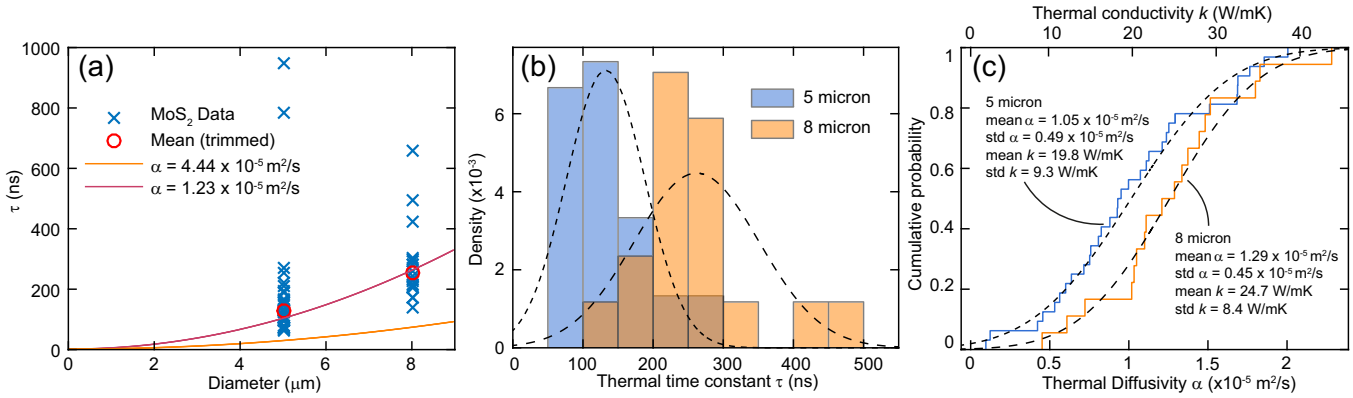

FIG. 2. (a) Thermal time constants as a function of diameter. Predictions using Eq. (4) are plotted with several values of k obtained from literature: $k = 23.3\ \mathrm{W\,m^{-1}\,K^{-1}}$ corresponding to $\alpha = 1.23 \times 10^{-5}\ \mathrm{m^2/s}$ [12] and $84\ \mathrm{W\,m^{-1}\,K^{-1}}$ to $\alpha = 4.44 \times 10^{-5}\ \mathrm{m^2/s}$ [18]. (b) Density plot of the thermal time constant for both diameters, drums with extremely large values of τ and low resonance frequency were excluded. (c) CDF (cumulative density function) of the thermal conductivity k estimated from the values of τ using $c_p = 373.5\ \mathrm{J\,kg^{-1}\,K^{-1}}$ and $\rho = 5060\ \mathrm{kg/m^3}$.

the specific heat, k the thermal conductivity, $\mathbf{x}$ is the position vector, and t is time. By separation of variables, and by using a lumped element model with a sinusoidal incident laser heat flux $P = P_{\mathrm{ac}} e^{i\omega t}$, Eq. (1) can be simplified, which results in a single relaxation time approximation for the time-dependent temperature:

$$C\frac{d\Delta T}{dt} + \frac{1}{R}\Delta T = P_{\mathrm{ac}} e^{i\omega t}, \tag{2}$$

where C is the heat capacity and R the thermal resistance. Below the resonance frequency, the mechanical deflection $z = z_\omega \mathrm{e}^{i\omega t}$ of the membrane is proportional to the temperature change, $z = A\Delta T$, such that it follows from Eq. (2) that [20,32]

$$z_\omega = \frac{A P_{\mathrm{ac}} R}{i\omega\tau + 1} = A P_{\mathrm{ac}} R \frac{1 - i\omega\tau}{1 + \omega^2\tau^2}, \tag{3}$$

where A is a proportionality constant that will be obtained by fitting and $\tau = RC$ the thermal time constant of the suspended drum.

The thermal time constant τ can be determined from the measured thermomechanical frequency response of the drum over several decades using the setup in Fig. 1(a). Figure 1(c) shows the real and imaginary part of the experimentally obtained frequency response from a MoS_2 drum with a diameter of 8 μm. It follows from Eq. (3) that the imaginary part of the response function has a maximum amplitude at $\omega\tau = 1$. This maximum is indeed observed at a cut-off frequency of $\omega_c = 2\pi \times 800$ kHz in Fig. 1(c), which is far below the membrane's lowest resonance frequency such that the relation $z_\omega = A\Delta T$ is valid. By fitting the imaginary part using Eq. (3), the thermal time constant of the membrane is determined to be $\tau = 1/\omega_c = 227$ ns. The resonance peaks were analyzed by fitting a harmonic oscillator model to the data, from which the resonance frequency and quality factor are found. Although both the real and imaginary parts of the response function fit well to Eq. (3), deviations around 300 kHz are observed, which are attributed to electrical crosstalk, most likely due to capacitive coupling to the optical table containing the experimental setup. Because the laser powers are low in these experiments, to prevent damage to the drums, the total optical signal on the photodiode is very low, making the system very susceptible to parasitic crosstalk. In Ref. [22], we show additional experiments on single-layer graphene that shows that at higher laser powers the feature disappears. The low-frequency data were excluded for the fit in order to prevent crosstalk from affecting the value of τ.

IV. RESULTS

Frequency response fits as shown in Fig. 1(c) are obtained on a total of 32 single-layer MoS_2 drums with a 5 μm diameter and 18 drums with an 8 μm diameter. Figure 2(a) shows the experimentally obtained values from all the drums as a function of drum size, and Fig. 2(b) shows a density plot for both diameters. Significant spread in the value of τ is found, even for drums of the same diameter. To exclude large effects of outliers, we only analyzed 80% of the samples with value τ closest to the mean and found $\bar{\tau} = 126$ ns for the 5 μm diameter drums and $\bar{\tau} = 253$ ns for the 8 μm drums.

Aubin derived an expression for the thermal time constant for a uniformly heated circular drum [33,34]:

$$\tau = \frac{a^2 \rho c_p}{\mu^2 k}, \tag{4}$$

where a is the drum radius, ρ the density, c_p the specific heat at constant pressure, and k the thermal conductivity of the material. For a uniformly heated drum, $\mu = 2.4048$ is the first root of the Bessel function $J_0(x)$. However, in the experiments, the membrane is heated by a focused laser spot in the center of the drum. We therefore use a numerical COMSOL model that adapts the value of μ by taking a point heat source in the center of the membrane. The measurement of the temperature is taken as the average temperature over the surface of the drum, since we expect the mechanical response to depend on the temperature field in the entire drum. From the simulations, it was found that $\mu^2 = 5.0$ is an accurate representation of the experiments. This should predict the value of k with an error less than 10% as long as $15 < k < 100\ \mathrm{W\,m^{-1}\,K^{-1}}$ and assuming that $c_p = 373.5\ \mathrm{J\,kg^{-1}\,K^{-1}}$

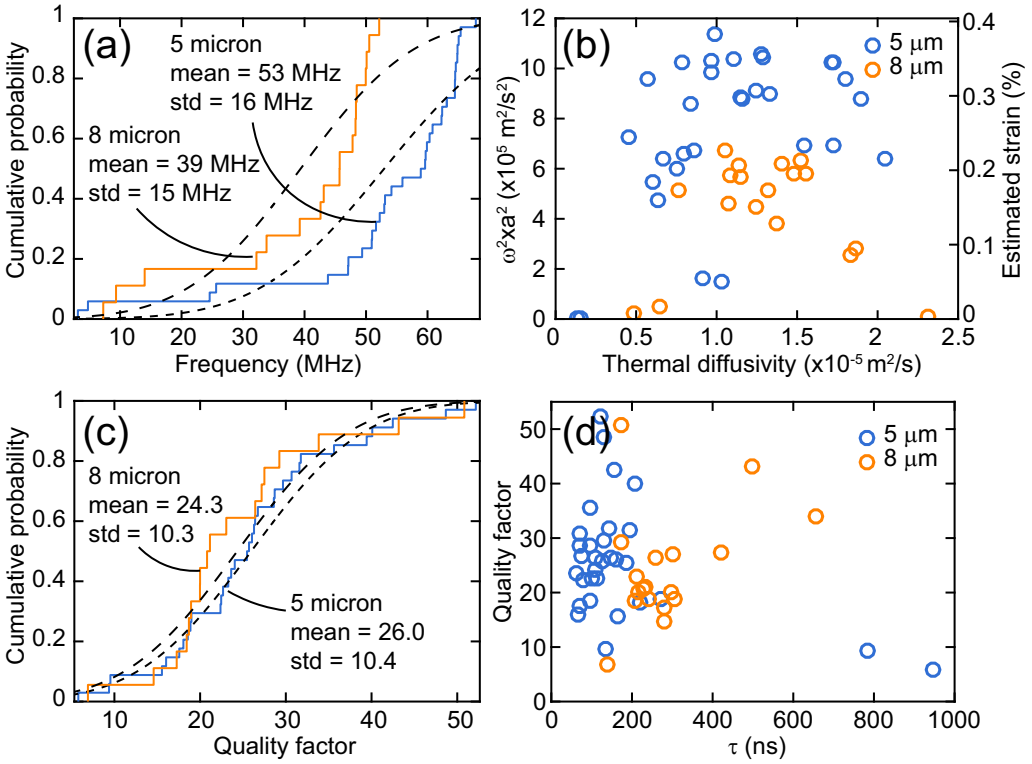

FIG. 3. Investigation of correlations between the mechanical and thermal properties. (a) CDF of the resonance frequency for both diameters. (b) Scatter plot with the thermal diffusivity on the horizontal axis and frequency times radius squared (which is proportional to tension) on the vertical axis. (c) CDF of the quality factor for both diameters. (d) Scatter plot with the thermal time constant on the horizontal and quality factor of resonance on the vertical axis.

(see Ref. [22]). Using Eq. (4), we can estimate the thermal diffusivity of MoS_2 $\alpha = k/\rho c_p$:

$$\alpha = \frac{a^2}{5\tau}. \tag{5}$$

This expression was used to estimate the thermal diffusivity for each drum as shown in Fig. 2(c). We find the diffusivity is slightly diameter-dependent with an average diffusivity $\bar{\alpha} = 1.05 \times 10^{-5}\,\mathrm{m^2/s}$ for the 5 μm drums and $\bar{\alpha} = 1.29 \times 10^{-5}\,\mathrm{m^2/s}$ for the 8 μm drums.

Based on known values of c_p and ρ of molybdenum disulfide at room temperature ($c_p = 373.5\ \mathrm{J\,kg^{-1}\,K^{-1}}$ and $\rho = 5060\ \mathrm{kg/m^3}$), we can estimate $k = a^2\rho c_p/(5\tau)$ from experimental values of τ. Figure 2(c) shows the cumulative density function (CDF) calculated for each drum. We find a mean of k, $\bar{k} = 19.8\ \mathrm{W\,m^{-1}\,K^{-1}}$ with a standard deviation of $9.3\ \mathrm{W\,m^{-1}\,K^{-1}}$ for the 5 μm drums and for the 8 μm drums we find $\bar{k} = 24.7\ \mathrm{W\,m^{-1}\,K^{-1}}$ with standard deviation $\sigma_k = 8.4\ \mathrm{W\,m^{-1}\,K^{-1}}$. We thus observe a considerable spread between devices. Moreover, most of the values of k found here are smaller compared to previous observations in literature that used exfoliated MoS_2 devices [17,18], but are larger than CVD MoS_2 values [19].

A. Comparison to the resonant properties

The transient mechanical characterization allows one to study whether the mechanical properties of the suspended drums are correlated to the thermal properties. This might be expected since the acoustic phonon velocities can be tension dependent, which would result in a correlation between the resonance frequency and the thermal diffusivity. Also, mechanical damping in MoS_2 due to defects could cause increased phonon scattering, which would lead to a lower thermal conductivity for drums with a low mechanical Q.

To study this, the resonance peaks were fitted by a harmonic oscillator model to extract the resonance frequency and the quality factor. The distribution of all the resonance frequencies is shown in Fig. 3(a) and the quality factors are shown in Fig. 3(c). We first investigate whether the thermal diffusivity is affected by strain in the resonator. The fundamental resonance frequency f of a circular drum resonator is given by

$$f = \frac{2.4048}{2\pi a}\sqrt{\frac{n_0}{\rho h}}, \tag{6}$$

where $h = 0.615\,\mathrm{nm}$ is the thickness of the drum and n_0 the tension in the membrane. From this, we deduce that $f^2a^2 \propto n_0$ if ρh is the same for each drum. Figure 3(b) shows a scatter plot of f^2a^2 versus the thermal diffusivity for each drum. The strain ϵ was estimated using the expression

$$\epsilon \approx \frac{n_0}{E_{2D}} = \frac{4\pi^2 f^2 a^2 \rho h}{2.4048^2 E_{2D}}, \tag{7}$$

where we assume the membrane has an ideal mass and the 2D Young's modulus E_{2D} was taken as 160 N/m [24,35]. No meaningful correlation between tension or strain and the thermal diffusivity could be uncovered in Fig. 3(b).

We further investigate whether the mechanical dissipation is related to the heat transport properties of these drums by examining the correlations to the quality factor. Figure 3(d) shows a scatter plot of the quality factor of resonance versus the thermal time constant. No significant correlation between the thermal time constant and the quality factor of resonance is found from the experimental data. The quality factor is nearly independent of diameter as shown in Fig. 3(c), we find $\bar{Q} = 26.0$ with standard deviation 10.4 for the 5 μm drums and $\bar{Q} = 24.3$ with standard deviation $\sigma_Q = 10.3$ for the 8 μm drums.

B. Phonon relaxation time and mean free path

The thermal conductivity can be expressed as $k \approx \rho c_p v \lambda$ [36], where v and λ are appropriately averaged phonon group velocity and mean free path, respectively. Substituting this expression in Eq. (4) gives

$$\tau = \frac{a^2}{5v\lambda} = \frac{a^2}{5v^2\tau_{ph}}, \tag{8}$$

where $\tau_{ph} = \lambda/v$ is the phonon relaxation time. We take the averaged velocity as $v \approx 300$ m/s based on calculations from several theoretical works [12,37,38] and use Eq. (8) to estimate τ_{ph} and λ. For the 5 μm drums, we find an average phonon relaxation time and mean free path of 116 ps and 34.9 nm, respectively. For the 8 μm drums, we find 143 ps and 43.2 nm. For both cases, we again find device-to-device variations due to the spread in the measured values of τ.

V. DISCUSSION

A. Comparison to single-layer graphene

In Fig. 4, we compare the experimentally obtained values of τ with experimentally obtained values of single-layer graphene (data from previous work in Ref. [20]) for drums with a 5 μm diameter. From the CDF in Fig. 4(a), it can be seen that both materials have a thermal time constant with the same order of magnitude. This is striking because even in the worst case scenario (CVD graphene with a lot of defects, $k \approx 600$ W m^{-1} K^{-1}) graphene should have a thermal diffusivity at least ten times higher than MoS_2. In this previous work, on single-layer graphene, we attributed the anomalous diameter dependence of τ to boundary effects that were limiting the heat transport. Since we only measured two diameters in this work, we cannot use diameter dependence to draw conclusions. Nevertheless, the values of τ on MoS_2 are in good agreement with the theory of diffusive heat transport. This can be seen by comparing the measured values of τ to the theoretical predictions from literature as shown in Fig. 2(a). Any effects of a thermal boundary resistance based on the measurements on MoS_2 are too small to be discerned. Molybdenum disulfide has a much lower thermal conductivity than graphene, which means that the intrinsic thermal resistance is more important than thermal resistance at the boundary of the drum if such a resistance is present at all in the case of MoS_2.

It is interesting to study the sign of the phase in Fig. 1(c): at low frequencies, the response is out-of-phase with the optical drive. We found that all the drums in this work show an out-of-phase response at low frequencies, in the case of graphene, we also found such a preference [20] where only a handful of graphene drums show an opposite phase. The optothermal drive works by modulation of the tension in the membrane [31] and some initial out-of-plane deflection is necessary in order for this to result in out-of-plane motion. Whether this deflection is up or down, determines the phase of the low-frequency response. Both graphene and MoS_2 thus have a preferred initial deflection. However, to determine whether this is up or down is difficult because this requires further characterization of the optical properties of the cavity, which determines the sign of dI/dx, the derivative of diode intensity I with respect to membrane position x [29].

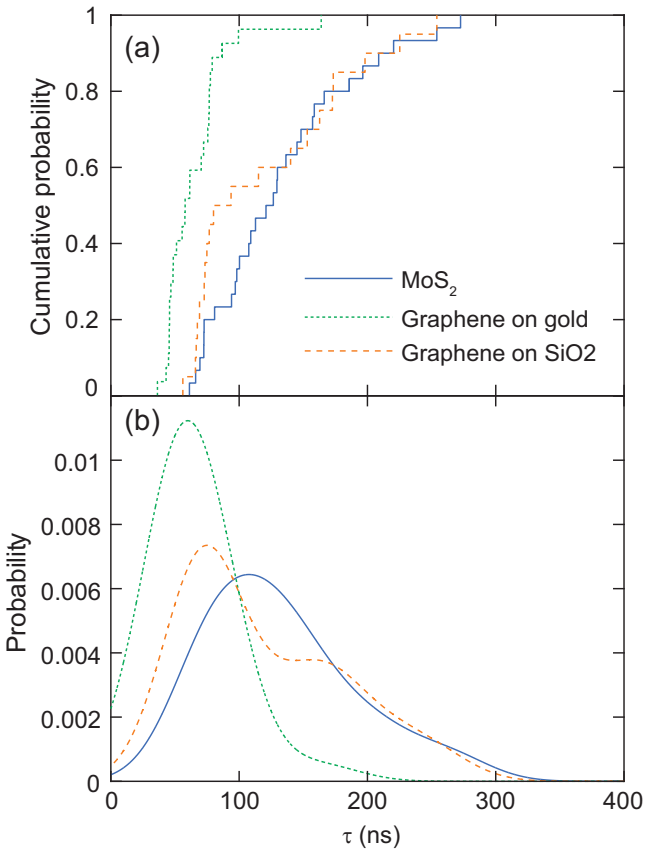

FIG. 4. (a) Cumulative probabilities from the experimental values of the thermal time constant in this work and for the case of single-layer graphene for drums with a 5 μm diameter. (b) Empirical distribution functions found by fitting a Kernel distribution with a 30 ns bandwidth to the data.

B. Relation between mechanical and thermal properties

We could not uncover any meaningful correlation between strain and the thermal diffusivity from the experimental data. The spread in the strain between the devices estimated from the resonance frequency is no more than 0.4%, which should result in a spread in the thermal conductivity of approximately 3% [39]. The measured device-to-device spread is significantly larger and strain-dependence is thus not the cause of the observed variations. It should be considered that the value of f^2a^2 could actually show spread between devices due to variations in the mass due to contamination. Since

contamination might affect the properties of 2D materials, atomic force microscopy measurements were performed to estimate the amount of residues as shown in Ref. [22]. We find a layer of contamination approximately 1 nm thick, indicating that the mass is underestimated and the variations in strain are actually larger than shown in Fig. 3(b). Upon removing the contamination using contact-mode atomic force microscopy (AFM) [40], we find the thermal time constant increases significantly by approximately 20%. This systematic error is considerably lower that the device-to-device spread in the thermal diffusivity observed in this work, which suggest that the effect of contamination on the measured values of τ is small.

C. Device-to-device spread

The observed device-to-device variations in τ might be attributed to variations in microscopic (point defects) and macroscopic imperfections between devices, that could alter the phonon relaxation times between devices explaining our result in Fig. 2(c). From calculations from the literature [37] using the Boltzmann transport equation for phonons, we would expect a mean free path of 316.5 nm for naturally occurring MoS_2. The significantly shorter mean free paths ($\sim$20 to 60 nm) found here might be related to our use of CVD MoS_2 rather than pristine exfoliated samples. Additional defects can increase the phonon scattering rate, lowering the phonon relaxation time and the mean free path. Also, the contamination on the samples found in Ref. [22] might be of influence, as was found in the case of graphene [41]. However, we show in Ref. [22] that removing the contamination did not significantly reduce the device-to-device spread, which suggests that its effect on τ is small. Most of the drums show a higher value of k than previous observations on CVD-grown MoS_2 [19], which could be related to differences in quality of the sample. The value of the mean free path shows that $\lambda \ll a$, this supports our notion that heat transport can be described by continuum models in these devices.

D. Specific heat

Given the arguments above, the significant spread in τ is most likely related to the scattering mechanisms. However, we cannot fully exclude the possibility that the heat capacity of the drums is responsible for the spread in τ. Little is known about potential mechanisms that can affect the specific heat of single-layered two-dimensional materials due to the lack of experimental data. However, the specific heat is most likely not very different from the bulk material since the number of vibrational degrees of freedom is the same. Also, the weak temperature dependence of the value of c_p is expected since the experiments are performed above the Debye temperature, therefore most degrees of freedom in the lattice are thermalized.

What we can conclude is that some of the literature values of k are impossible to have occurred in our measurements, since they would violate the Petit-Dulong limit ($c_p = 468.8\ \mathrm{J\,kg^{-1}\,K^{-1}}$). The fastest 5 μm diameter drum has $\tau = 61$ ns, which means that there is a limit on the thermal conductivity: $k \leqslant 48\ \mathrm{W\,m^{-1}\,K^{-1}}$. For the fastest 8 μm diameter drum, $\tau = 138$ ns and it is impossible that the thermal conductivity of this drum exceeded 55 $\mathrm{W\,m^{-1}\,K^{-1}}$. Therefore the highest reported value of $k = 84\ \mathrm{W\,m^{-1}\,K^{-1}}$ [18], cannot have occurred in the drums used in this study. Also, the reported value of $k = 34.5\ \mathrm{W\,m^{-1}\,K^{-1}}$ [17], would implicate that the Petit-Dulong limit is violated in most of the devices.

The most representative study, since it uses both CVD MoS_2 and conducted the experiment in vacuum, is $k = 13.3 \pm 1.4\ \mathrm{W\,m^{-1}\,K^{-1}}$ [19]. Using this value, we can use the experimentally obtained values of τ to estimate the specific heat of MoS_2. For the 5 μm drums, we find $c_p = 278 \pm 118\ \mathrm{J\,kg^{-1}\,K^{-1}}$ and for the 8 μm drums we find $c_p = 215 \pm 73\ \mathrm{J\,kg^{-1}\,K^{-1}}$. The errors represent the standard deviation due to the large device-to-device spread, nevertheless, this analysis suggests that most of the devices have a specific heat that is significantly lower than the bulk value. Future work can combine the transient characterization with existing methods, such as Raman spectroscopy or electrical heaters, to extract the thermal resistance R. In that case, the heat capacity C can be derived and provide more accurate measurements on the specific heat of 2D materials. The transient characterization thus provides a means to perform calorimetry on suspended 2D materials.

VI. CONCLUSION

We measured the thermal time constants of suspended monolayer molybdenum disulfide drums. In contrast to previous measurements on single-layer graphene, we find that the values of τ are in agreement with the classical Fourier theory of heat transport. From the values of τ, we can estimate the thermal conductivity to be between 10 and 40 $\mathrm{W\,m^{-1}\,K^{-1}}$, which is lower than previous measurements on exfoliated MoS_2 but in agreement with measurements on CVD-grown MoS_2. Significant device-to-device variation in thermal time constants is observed. This variation is not correlated to the resonance frequency or Q-factor of the membranes, which shows that mechanisms that determine the macroscopic damping are probably not responsible for the observed spread. We therefore conclude that the variations in thermal diffusivity are caused by microscopic defects that have a large impact on phonon scattering but do not affect the resonance frequency and damping of the membrane's lowest eigenmode. The method can be used to estimate the specific heat of single-layer MoS_2, with our results suggesting its value might be lower than the bulk value. Future work can combine this technique with existing thermal conductivity measurements to perform calorimetry on suspended 2D materials, enabling one to determine whether the specific heat of 2D materials is equal to its bulk value.

ACKNOWLEDGMENTS

This work is part of the research programme Integrated Graphene Pressure Sensors (IGPS) with Project No. 13307, which is financed by the Netherlands Organisation for Scientific Research (NWO). The research leading to these results also received funding from the European Union's

Horizon 2020 research and innovation programme under grant agreement No 785219 Graphene Flagship. J.S.B. and D.L. were funded by the National Science Foundation (NSF) grant No. 1706322 (CBET: Bioengineering of Channelrhodopsins for Neurophotonic and Nanophotonic Applications) and Boston University.

[1] K. F. Mak, C. Lee, J. Hone, J. Shan, and T. F. Heinz, Atomically Thin MoS_2: A New Direct-Gap Semiconductor, Phys. Rev. Lett. **105**, 136805 (2010).

[2] A. Splendiani, L. Sun, Y. Zhang, T. Li, J. Kim, C.-Y. Chim, G. Galli, and F. Wang, Emerging photoluminescence in monolayer MoS_2, Nano Lett. **10**, 1271 (2010).

[3] G. Eda, H. Yamaguchi, D. Voiry, T. Fujita, M. Chen, and M. Chhowalla, Photoluminescence from chemically exfoliated MoS_2, Nano Lett. **11**, 5111 (2011).

[4] A. Castellanos-Gomez, R. van Leeuwen, M. Buscema, H. S. J. van der Zant, G. A. Steele, and W. J. Venstra, Single-layer MoS_2 mechanical resonators, Adv. Mater. **25**, 6719 (2013).

[5] S. Bertolazzi, J. Brivio, and A. Kis, Stretching and breaking of ultrathin MoS_2, ACS nano **5**, 9703 (2011).

[6] B. Radisavljevic, A. Radenovic, J. Brivio, V. Giacometti, and A. Kis, Single-layer MoS_2 transistors, Nat. Nanotechnol. **6**, 147 (2011).

[7] Z. Yin, H. Li, H. Li, L. Jiang, Y. Shi, Y. Sun, G. Lu, Q. Zhang, X. Chen, and H. Zhang, Single-layer MoS_2 phototransistors, ACS nano **6**, 74 (2011).

[8] M. Buscema, J. O. Island, D. J. Groenendijk, S. I. Blanter, G. A. Steele, H. S. J. van der Zant, and A. Castellanos-Gomez, Photocurrent generation with two-dimensional van der Waals semiconductors, Chem. Soc. Rev. **44**, 3691 (2015).

[9] M. Buscema, G. A. Steele, H. S. J. van der Zant, and A. Castellanos-Gomez, The effect of the substrate on the Raman and photoluminescence emission of single-layer MoS_2, Nano Res. **7**, 561 (2014).

[10] M. Buscema, M. Barkelid, V. Zwiller, H. S. J. van der Zant, G. A. Steele, and A. Castellanos-Gomez, Large and tunable photothermoelectric effect in single-layer MoS_2, Nano Lett. **13**, 358 (2013).

[11] X. Liu, G. Zhang, Q.-X. Pei, and Y.-W. Zhang, Phonon thermal conductivity of monolayer MoS_2 sheet and nanoribbons, Appl. Phys. Lett. **103**, 133113 (2013).

[12] Y. Cai, J. Lan, G. Zhang, and Y.-W. Zhang, Lattice vibrational modes and phonon thermal conductivity of monolayer MoS_2, Phys. Rev. B **89**, 035438 (2014).

[13] X. Wei, Y. Wang, Y. Shen, G. Xie, H. Xiao, J. Zhong, and G. Zhang, Phonon thermal conductivity of monolayer MoS_2: A comparison with single layer graphene, Appl. Phys. Lett. **105**, 103902 (2014).

[14] W. Li, J Carrete, and N. Mingo, Thermal conductivity and phonon linewidths of monolayer MoS_2 from first principles, Appl. Phys. Lett. **103**, 253103 (2013).

[15] J.-W. Jiang, H. S. Park, and T. Rabczuk, Molecular dynamics simulations of single-layer molybdenum disulphide (MoS_2): Stillinger-Weber parametrization, mechanical properties, and thermal conductivity, J. Appl. Phys. **114**, 064307 (2013).

[16] N. A. Lanzillo, A. Glen Birdwell, M. Amani, F. J. Crowne, P. B. Shah, S. Najmaei, Z. Liu, P. M. Ajayan, J. Lou, M. Dubey, S. K. Nayak, and T. P. O'Regan, Temperature-dependent phonon shifts in monolayer MoS_2, Appl. Phys. Lett. **103**, 093102 (2013).

[17] R. Yan, J. R. Simpson, S. Bertolazzi, J. Brivio, M. Watson, X. Wu, A. Kis, T. Luo, A. R. Hight Walker, and H. G. Xing, Thermal conductivity of monolayer molybdenum disulfide obtained from temperature-dependent Raman spectroscopy, ACS nano **8**, 986 (2014).

[18] X. Zhang, D. Sun, Y. Li, G.-H. Lee, X. Cui, D. Chenet, Y. You, T. F. Heinz, and J. C. Hone, Measurement of lateral and interfacial thermal conductivity of single- and bilayer MoS_2 and $MoSe_2$ using refined optothermal Raman technique, ACS Appl. Mater. Interfaces **7**, 25923 (2015).

[19] J. J. Bae, H. Y. Jeong, G. H. Han, J. Kim, H. Kim, M. S. Kim, B. H. Moon, S. C. Lim, and Y. H. Lee, Thickness-dependent in-plane thermal conductivity of suspended MoS_2 grown by chemical vapor deposition, Nanoscale **9**, 2541 (2017).

[20] R. J. Dolleman, S. Houri, D. Davidovikj, S. J. Cartamil-Bueno, Y. M. Blanter, H. S. J. van der Zant, and P. G. Steeneken, Optomechanics for thermal characterization of suspended graphene, Phys. Rev. B **96**, 165421 (2017).

[21] B. R. Matis, B. H. Houston, and J. W. Baldwin, Energy dissipation pathways in few-layer MoS_2 nanoelectromechanical systems, Sci. Rep. **7**, 5656 (2017).

[22] See Supplemental Material at http://link.aps.org/supplemental/10.1103/PhysRevMaterials.2.114008 for the COMSOL model used to derive Eq. (4), additional discussion on the electrical crosstalk visible in Fig. 1(c) and AFM characterization of contamination on the sample.

[23] J. W. Suk, A. Kitt, C. W. Magnuson, Y. Hao, S. Ahmed, J. An, A. K. Swan, B. B. Goldberg, and R. S. Ruoff, Transfer of CVD-grown monolayer graphene onto arbitrary substrates, ACS nano **5**, 6916 (2011).

[24] D. Lloyd, X. Liu, N. Boddeti, L. Cantley, R. Long, M. L. Dunn, and J. S. Bunch, Adhesion, stiffness, and instability in atomically thin MoS_2 bubbles, Nano Lett. **17**, 5329 (2017).

[25] D. Lloyd, X. Liu, J. W. Christopher, L. Cantley, A. Wadehra, B. L. Kim, B. B. Goldberg, A. K. Swan, and J. S. Bunch, Band gap engineering with ultralarge biaxial strains in suspended monolayer MoS_2, Nano Lett. **16**, 5836 (2016).

[26] D. Sercombe, S. Schwarz, O. Del Pozo-Zamudio, F. Liu, B. J. Robinson, E. A. Chekhovich, I. I. Tartakovskii, O. Kolosov, and A. I. Tartakovskii, Optical investigation of the natural electron doping in thin MoS_2 films deposited on dielectric substrates, Sci. Rep. **3**, 3489 (2013).

[27] N. Scheuschner, O. Ochedowski, A.-M. Kaulitz, R. Gillen, M. Schleberger, and J. Maultzsch, Photoluminescence of free-standing single- and few-layer MoS_2, Phys. Rev. B **89**, 125406 (2014).

[28] H. Li, Q. Zhang, C. C. R. Yap, B. K. Tay, T. H. T. Edwin, A. Olivier, and D. Baillargeat, From bulk to monolayer MoS_2: evolution of Raman scattering, Adv. Funct. Mater. **22**, 1385 (2012).

[29] R. J. Dolleman, D. Davidovikj, H. S. J. van der Zant, and P. G. Steeneken, Amplitude calibration of 2D mechanical resonators by nonlinear optical transduction, Appl. Phys. Lett. **111**, 253104 (2017).

[30] J. S. Bunch, A. M. Van Der Zande, S. S. Verbridge, I. W. Frank, D. M. Tanenbaum, J. M. Parpia, H. G. Craighead, and P. L. McEuen, Electromechanical resonators from graphene sheets, Science **315**, 490 (2007).

[31] R. J. Dolleman, S. Houri, A. Chandrashekar, F. Alijani, H. S. J. van der Zant, and P. G. Steeneken, Opto-thermally excited multimode parametric resonance in graphene membranes, Sci. Rep. **8**, 9366 (2018).

[32] C. Metzger, I. Favero, A. Ortlieb, and K. Karrai, Optical self cooling of a deformable Fabry-Perot cavity in the classical limit, Phys. Rev. B **78**, 035309 (2008).

[33] K. L. Aubin, Radio frequency nano/microelectromechanical resonators: Thermal and nonlinear dynamics studies, Ph.D. dissertation, Cornell University Ithaca, NY, 2004.

[34] J. S. Bunch, Mechanical and electrical properties of graphene sheets, Ph.D. dissertation, Cornell University Ithaca, NY, 2008.

[35] K. Liu, Q. Yan, M. Chen, W. Fan, Y. Sun, J. Suh, D. Fu, S. Lee, J. Zhou, S. Tongay, J. Ji, J. B. Neaton, and J. Wu, Elastic properties of chemical-vapor-deposited monolayer MoS_2, WS_2, and their bilayer heterostructures, Nano Lett. **14**, 5097 (2014).

[36] E. Pop, V. Varshney, and A. K. Roy, Thermal properties of graphene: Fundamentals and applications, MRS Bull. **37**, 1273 (2012).

[37] B. Peng, H. Zhang, H. Shao, Y. Xu, X. Zhang, and H. Zhu, Towards intrinsic phonon transport in single-layer MoS_2, Ann. Phys. **528**, 504 (2016).

[38] Y. Gan and H. Zhao, Chirality and vacancy effect on phonon dispersion of MoS_2 with strain, Phys. Lett. A **380**, 745 (2016).

[39] L. Zhu, T. Zhang, Z. Sun, J. Li, G. Chen, and S. A. Yang, Thermal conductivity of biaxial-strained MoS_2: Sensitive strain dependence and size-dependent reduction rate, Nanotechnology **26**, 465707 (2015).

[40] A. M. Goossens, V. E. Calado, A. Barreiro, K. Watanabe, T. Taniguchi, and L. M. K. Vandersypen, Mechanical cleaning of graphene, Appl. Phys. Lett. **100**, 073110 (2012).

[41] I. Jo, M. T. Pettes, L. Lindsay, E. Ou, A. Weathers, A. L. Moore, Z. Yao, and L. Shi, Reexamination of basal plane thermal conductivity of suspended graphene samples measured by electro-thermal micro-bridge methods, AIP Adv. **5**, 053206 (2015).